Modeling and Experimental Validation of an Islanded No-Inertia Microgrid Site

Bonfiglio, Andrea; Delfino, Federico; Labella, Alessandro; Mestriner, Daniele; Pampararo, Fabio; Procopio, Renato; Guerrero, Josep M.

Published in:
IEEE Transactions on Sustainable Energy

DOI (link to publication from Publisher):
10.1109/TSTE.2018.2816401

Publication date:
2018

Document Version
Accepted author manuscript, peer reviewed version

This article has been accepted for publication in a future issue of this journal, but has not been fully edited. Content may change prior to final publication. Citation information: DOI 10.1109/TSTE.2018.2816401, IEEE Transactions on Sustainable Energy

Modeling and Experimental Validation of an Islanded No-Inertia Microgrid Site

Andrea Bonfiglio *Member, IEEE*, Federico Delfino, *Member, IEEE*, Alessandro Labella, *Student Member, IEEE*, Daniele Mestriner, *Student Member, IEEE*, Fabio Pampararo, Renato Procopio, *Senior Member, IEEE*, and Josep M. Guerrero, *Fellow, IEEE*

***Abstract* — The paper proposes a simple but effective model for no-inertia microgrids suitable to represent the instantaneous values of its meaningful electric variables, becoming a useful platform to test innovative control logics and energy management systems. The proposed model is validated against a more detailed microgrid representation implemented in the electromagnetic simulator PSCAD-EMTDC and then against experimental data collected on the University of Genoa test bed facility. Recorded data highlight a good trade-off in matching the results of the proposed model, confirming its suitability to be used for the preliminary testing of new control logics for islanded microgrids.**

***Index Terms* — Smart grids, Power system modelling, Islanding, Microgrids, System validation**

NOMENCLATURE

$\dot{V}_k$	AC voltage of *k-th* power generating unit.
$V_{DC,k}$	DC voltage of *k-th* power generating unit.
m_k	Modulation index of *k-th* power generating unit.
ψ_k	A primitive of *k-th* power generating unit frequency.
φ_k	Phase shift of *k-th* power generating unit.
ω_k	Frequency of *k-th* power generating unit.
$P_{AC,k}$	AC active power of *k-th* power generating unit.
$\dot{I}_k$	AC current of *k-th* power generating unit.
Y_E	Extended admittance matrix.
$\dot{\boldsymbol{V}}_{\boldsymbol{L}}$	Load bus voltage vector
G_{ki}	Conductance of (*k*,*i*) element of Y_E.
B_{ki}	Susceptance of (*k*,*i*) element of Y_E.
C_k	DC-link capacitance of *k-th* power generating unit.
$P_{DC,k}$	DC active power of *k-th* power generating unit.
N	Number of the microgrid power generating units.
N_L	Number of load buses.
N_{PV}	Number of Photovoltaic (PV) generating units.
N_{ST}	Number of Storage (ST) generating units.
$V_{PV,r}$	DC voltage of *r-th* PV unit.
$I_{PV,r}$	DC current of *r-th* PV unit.
α	PV system solar irradiance.
I_{sc}	PV panels short circuit current.
$v_{max/min}$	PV unit maximum (minimum) open circuit voltage.
b	PV units shape factor.
$\tau_{v(I)}$	PV panels voltage (current) coefficient.
T	PV panels temperature.
$L_{ST,n}$	DC inductance of *n-th* ST unit.
$R_{int,n}$	Battery internal resistance of *n-th* ST unit.
SOC_n	State of charge of *n-th* ST unit.
E_n	No load voltage of *n-th* ST unit.
$V_{batt,n}$	Battery terminal voltage of *n-th* ST unit.
NCC_n	Rated current capacity of *n-th* ST unit.
$K_{ST,n}$	DC/DC converter gain of *n-th* ST unit.
$I_{ST,n}$	DC current of *n-th* ST unit.
$R_{se,k}$	Series filter resistance of *k-th* power generating unit.
$L_{se,k}$	Series filter inductance of *k-th* power generating unit.
$R_{sh,k}$	Shunt filter resistance of *k-th* power generating unit.
$L_{sh,k}$	Shunt filter inductance of *k-th* power generating unit.
$C_{sh,k}$	Shunt filter capacitance of *k-th* power generating unit.

I. INTRODUCTION

MICROGRIDS (MGs) are one of the most promising architectures for power systems that are currently attracting the attention of researchers and industries of the sector thanks to their potential to face the necessity of the future electricity system with advanced and efficient Energy Management Systems (EMSs) [1, 2] and innovative control strategies [3, 4]. Among the various MG configurations, off-grid (or islanded) ones are expected to provide a significant impact on the flexibility and resiliency of the electricity system. Islanded MGs will of course allow the possibility of electrifying rural areas [5] but also improving the secure operation of the main electricity system due to the possibility of connecting or disconnecting them from the main grid in accordance to the needs of the Distribution or Transmission System Operator [6]. A particularly interesting case is the one in which all power sources are connected to the MG by means of power electronic devices (from now on "no-inertia MGs"). Nevertheless, the management, control and fault detection of such MGs is quite challenging due to the different dynamics behaviour with respect to the ones characterized by an inertial frequency response and due to the limited contribution to short circuit current provided by power electronic devices [7].

The interest in islanded MGs is witness by the relevant amount of work done by researchers in order to make this configuration performing and reliable; for example in [8] a revision of the traditional power sharing strategy is extended to islanded MGs, while in [9] a novel approach to voltage and frequency control for islanded MGs is discussed.

Besides the strong effort of researchers in order to find suitable and more and more efficient solutions to manage and control islanded no-inertia MGs, the attention cannot drift away from the needs of industries that have to receive and implement the solutions proposed by the academic world. Usually, industries require simple but effective tools to test and verify the complacencies of their products with the system operator requirements [10] or with the customer technical specifications [11]. This is because many companies do not have suitable tools and resources to develop detailed and complex power system models (licensed software are very expensive and resources are usually focused on design and implementation rather than research and development).

Attempts to define suitable simplified models for MGs can be found in [12] where the authors propose a linearized representation of a MG in both islanded and grid-tied configurations. The main disadvantage of [12] lays in the fact

that a linear model of a non-linear system requires further linearization around the system working point. Moreover, the proposed model also includes the specific control strategy of the MG converter, thus it is not suitable for the testing and validation of alternative MG control approaches.

For this reason, the first aim of the present paper is to define a simple, but effective model for no-inertia islanded MGs expressed in terms of a system of Ordinary Differential Equations (ODEs) capable of capturing all the dynamics of the involved electric quantities with a reduced set of input parameters. The proposed model keeps the system non-linearity and assumes the control input of the MG converters as its own inputs in order to be interfaced with any proposed control strategy. Moreover, it does not need any specific licensed software to be implemented and requires a limited CPU effort to run. The proposed model differs from the well-known Dynamic Phasor modelling [13, 14] in terms of considering the relationships among AC quantities as steady-state ones. On the other hand, DC dynamics are considered, so that any DC inductor or capacitor gives origin to one differential equation. AC variations are consequent to the variation of the DC quantities by means of the interfacing converters. These features lead to a Simplified Model (SM) with a reduced number of equations, particularly useful to test any kind of MG control architecture. Moreover, as will be detailed later on, the SM formulation is applicable to any generation mix of no-inertia MGs in a very flexible way.

Since the proposed SM is intended to fill the gap between theoretical research and the actual deployment of innovative control strategies for islanded, no-inertia MGs, an experimental validation of its performances would be of great value. On this topic, experimental validations on real MG infrastructures are very limited in literature. The majority of experimental validations are performed on laboratory prototypes of small scale converters or emulated MG configurations (e.g. [15, 16]). In other works, small converter prototypes are interfaced with real time digital simulators achieving an hybrid configuration (the so called Hardware In the Loop technique) [17, 18]. Nevertheless, the results of a validation on a full-scale, no-inertia MG is still missing due to the limited number of facilities designed for research purposes.

In order to fill this lack of experimental validations for islanded no-inertia MGs, the present article also aims at providing a validation of the proposed SM on a real MG. The test bed facility is the experimental infrastructure of the University of Genoa called the Smart Polygeneration Microgrid (SPM), a Low Voltage (LV) no-inertia test bed microgrid commissioned in 2014 and tested in islanded configuration at the beginning of 2017. In order to better understand the impact of the SM simplifying assumptions on the eventual deviations of its outputs from measurements, the results of the proposed SM and the experimental measurement are also compared against a complete implementation of the SPM islanded portion in the electromagnetic simulator PSCAD-EMTDC [19].

The paper is organized as follows: Section II details the methodological approach for the application of the proposed SM to a generic no-inertia MG while Section III presents the University of Genoa test bed MG, highlighting the characteristic of the MG portion designed to be islanded. Section IV describes the PSCAD implementation of the SPM islanded portion, Section V provides the definition of all the parameters needed to feed the SM and the PSCAD one on the basis of the SPM data. Finally, Section VI reports the results of the SM validation followed by some conclusive remarks in Section VII.

II. The Simplified Model

As specified in the introduction, the aim of the present paper is that of providing a simplified and flexible representation of no-inertia islanded MGs for testing and validation purposes of innovative control and energy management strategies. The proposed approach is based on a 1st harmonic model and is represented by of a set of ODEs under the following main assumptions:

1. The AC side portion of the MG is supposed to be at steady-state (assuming that both the angular frequencies of the sources and their voltages amplitude can vary), while all the DC dynamics are fully considered;
2. Power electronics converters models neglect higher order harmonics;
3. The shunt sections of inverters AC filters are neglected;
4. AC loads are represented by an algebraic current/voltage law in order to account for a wider set of load types (constant impedance, constant power and so one).

This last hypothesis leads to the definition of a voltage dependent network extended admittance matrix (see Appendix A) that does not allow to obtain an ODE system written in the normal form. All the details about how to numerical solve the resulting mixed differential/algebraic system can be found in Appendix B.

Let us assume that the MG is composed by N power generating units and N_L load buses and let us use the index k to represent the generic *k-th* inverter. The overall schematic representation of the off-grid MG considered for the SM is depicted in Fig. 1.

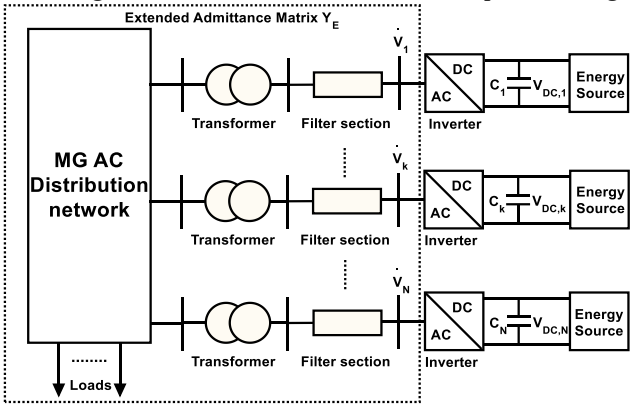

Fig. 1. MG layout considered for the definition of the SM.

For the generic *k-th* inverter, under the assumptions of the SM, it is possible to write the AC, line to ground voltage $\dot{V}_k$ as [20]:

$$\dot{V}_k(t) = \frac{m_k(t)}{2\sqrt{2}} V_{DC,k}(t) e^{j\delta_k(t)} \tag{1}$$

assuming that the *k-th* inverter is working in its linear operational range and defining the corresponding angle δ_k as:

$$\delta_k(t) = \psi_k(t) + \varphi_k(t) \tag{2}$$

where:

$$\frac{d\,\psi_k(t)}{dt} = \omega_k(t) \tag{3}$$

being ω_k and φ_k the angular frequency and the phase shift of the *k-th* converter, respectively. Thus, the active power injected by the *k-th* power generating unit into the AC grid is given by:

$$P_{AC,k} = 3\,\mathrm{Re}\left\{\dot{V}_k \dot{I}_k^*\right\} = 3\,\mathrm{Re}\left\{\dot{V}_k \sum_{i=1}^{N}\left(\dot{Y}_{E,ki}^*\left(\dot{\mathbf{V}}_L\right)\dot{V}_i^*\right)\right\} \tag{4}$$

where $\left[\dot{\mathbf{V}}_L\right] = \left[\dot{V}_{L1}..\dot{V}_{LN_L}\right]^T$ being $\dot{V}_{Li}$ the *i-th* load bus voltage and $\dot{Y}_{E,ki}^*\left(\dot{\mathbf{V}}_L\right)$ is the (*k*,*i*) element of the load voltage dependent extended admittance matrix $\boldsymbol{Y_E}$ defined in appendix A. Indicating with $G_{ki}\left(\dot{\mathbf{V}}_L\right)$ and $B_{ki}\left(\dot{\mathbf{V}}_L\right)$ $\dot{Y}_{E,ki}\left(\dot{\mathbf{V}}_L\right)$ real and imaginary part, it is possible rewriting (4) as:

$$P_{AC,k} = 3\frac{m_k V_{DC,k}}{8}\sum_{i=1}^{N}\left\{m_i V_{DC,i}\left[\begin{array}{l}\cos\left(\delta_k-\delta_i\right)G_{ki}\left(\dot{\mathbf{V}}_L\right)+\\ +\sin\left(\delta_k-\delta_i\right)B_{ki}\left(\dot{\mathbf{V}}_L\right)\end{array}\right]\right\}. \tag{5}$$

On the DC side of the inverter a capacitor C_k is connected with the aim of supporting the DC inverter voltage during power transients. The capacitor power balance can be written as:

$$C_k V_{DC,k}\frac{dV_{DC,k}}{dt} = P_{DC,k} - P_{AC,k} \tag{6}$$

$P_{DC,k}$ being the power injected by the *k-th* energy source at the DC link. $P_{DC,k}$ can be calculated entering into the details of the specific source supplying the inverter (e.g. ST units, PV plants, wind turbines, microturbines and so on). Since the aim of the present paper is not only to propose the SM but also to assess its performances and accuracy by means of an experimental validation campaign on a real test bed, our attention is now focused in recalling the detailed models for the generation sources that are included in the islanded portion of the University of Genoa SPM, i.e. PV and ST units. Nevertheless, this does not imply any loss of generality since one can extend the proposed methodology to different power sources simply providing a suitable characterization of the corresponding DC power $P_{DC,k}$. For example, for a wind power plant one has that the power at the DC side of the machine side converter can be calculated as a function of the wind speed v_w, the wind generator rotor speed ω_{WT} and the blades pitch angle β [21]. Thus, one can integrate this kind of power generation in the proposed SM implementing:

$$P_{DC,k} = f\left(v_w, \omega_{WT}, \beta\right). \tag{7}$$

If, on the other hand, a microturbine generating unit is concerned, its DC power is going to be written as a suitable function of the intake of feeding gas [22].

From now on, let us assume that the MG is composed by N_{PV} PV generating units and N_{ST} ST generating units. In the following, index *r* is used as reference for the generic PV generating unit and index *n* is used as reference for the generic ST one. PV units are described according to their current-voltage curve depending on the solar irradiance [23]:

$$I_{PV,r}\left(V_{PV,r}\right) = \alpha I_{sc}\tau_I(T)\left[\frac{1-e^{\frac{v_{PV,r}}{b\left(1+\frac{v_{max}-v_{min}}{v_{max}}\frac{\alpha-\alpha_{max}}{\alpha_{max}-\alpha_{min}}\right)\left(v_{max}+\tau_v(T)\right)}-\frac{1}{b}}}{1-e^{-1/b}}\right] \tag{8}$$

where α is the is the *p.u.* irradiance referred to 1000 W/m^2, I_{sc} is the short circuit current, v_{max} and v_{min} are respectively the maximum and minimum open circuit voltage corresponding to the maximum and minimum irradiation α_{max} and α_{min}, and *b* is a shape factor to be defined in order to match the specific datasheet Maximum Power Point (MPP) parameters (subscript *r* is omitted for the specific description of the PV panels model for the sake of readability). Since the DC voltage produced by the PV plant is connected to the DC side of the inverter, for the generic *r-th* PV unit the voltage $V_{PV,r}$ is the same as the DC inverter voltage $V_{DC,r}$, thus allowing us to write the DC power $P_{DC,r}$ to be inserted in (6) as:

$$P_{DC,r} = V_{DC,r} I_{PV,r}\left(V_{DC,r}\right) \tag{9}$$

The generic *n-th* ST is modelled as a non-ideal DC voltage generator representing the battery units connected to the DC side of the inverter by means of an intermediate DC/DC chopper in buck-boost configuration. The DC/DC converter is needed in order to keep a constant voltage at the DC side of the converter while the buck-boost configuration allows a bi-directional power flow. Between the battery and the DC/DC converter a series inductor is considered, $L_{ST,n}$, in order to operate the DC/DC converter also in step-up configuration. The ST equivalent circuit is depicted in Fig. 2.

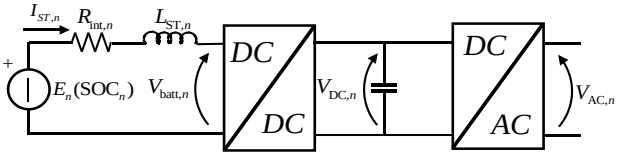

Fig. 2. Schematic circuital representation of the generic *n-th* ST unit.

The battery is represented by a Thevenin equivalent where the value of the voltage generator, namely E_n, is dependent on its state of charge (SOC_n). This dependency can be expressed by means of a 6th order polynomial in the form:

$$E_n\left(SOC_n\right) = \sum_{i=0}^{6} a_i \cdot SOC_n^{\,i} \tag{10}$$

The values of a_i coefficients vary in accordance to the specific battery technology (details on the ST modelling are available in [24]). Neglecting the dependence of the state of charge on the temperature (which is reasonable for the SPM battery technologies as specified in [24]), the DC voltage provided at the battery terminals, $V_{batt,n}$, can be then written as:

$$V_{batt,n}\left(SOC_n, I_{ST,n}\right) = E_n\left(SOC_n\right) - I_{ST,n}R_{int,n} \tag{11}$$

where $R_{int,n}$ is the battery internal resistance. SOC_n is related to the ST current $I_{ST,n}$ by:

$$\frac{d\,SOC_n}{dt} = -\frac{I_{ST,n}}{NCC_n} \tag{12}$$

where NCC_n is the nominal current capacity of the *n-th* ST. Considering a first harmonic representation for the DC/DC

converter too, it is possible writing the state equation of the *n-th* ST inductor as:

$$L_{ST,n}\frac{dI_{ST,n}}{dt} = E_n\left(SOC_n\right) - R_{\text{int},n}I_{ST,n} - \frac{V_{DC,n}}{K_{ST,n}} \tag{13}$$

where $K_{ST,n}$ is the DC/DC converter gain. The DC/DC controller has the aim of keeping constant the ST DC link voltage [20]. For the *n-th* ST unit, one can now define the DC power to be used in (6) as:

$$P_{DC,n} = \frac{V_{DC,n}I_{ST,n}}{K_{ST,n}} \tag{14}$$

Equations (2)-(3), (5)-(14) represent the system behaviour and completely describe the DC dynamics of the MG. The modelling of the network with the extended admittance matrix allows accounting for the influence of the network topology on the AC side power flows. The inputs of the proposed SM can be divided into two categories: *(i)* physical inputs that depend on the specific energy source (wind speed, solar irradiance, fuel, etc.) and *(ii)* control inputs that are the inverters modulation index m_k, frequency ω_k and phase φ_k. Such inputs are provided by the MG controller according to the specific control strategy. Since the scope of the work is to propose a SM of the MG power system to be interfaced with any control logic *(i)* and *(ii)* are going to be the boarder signals of the proposed modelling. Nevertheless, since a comparison with the experimental data collected at the University of Genoa test bed MG will be presented to validate the proposed approach, a brief description of the SPM control system and its implementation in the proposed simulations will be detailed in Section VI.

III. Experimental Validation on the Smart Polygeneration Microgrid

Experimental validation of the proposed SM is going to be done at the University of Genoa SPM test bed facility. The SPM is a LV (400 V line-line) AC smart MG located in the Savona Campus of Genoa University. The SPM was unveiled in 2010 with the aim of providing a test bed facility for the definition and validation of innovative EMS, control logics and distributed energy resources integration in LV MGs in both grid connected and islanded configurations. The SPM includes a number of heterogeneous energy sources, such as Combined Heat and Power, gas microturbines, PV power plants, Concentrating Solar Power and two technologies of electric ST devices, Li-ion and Sodium-Nickel. The SPM is monitored and controlled by means of a dedicated EMS, developed by the University of Genoa researchers [22] when operating in grid connected configuration and installed in a dedicated control unit located in the SPM control room. A more detailed description of the SPM can be found in [25].

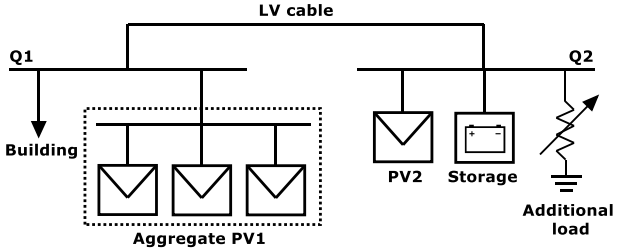

Fig. 3. An overview of the islanded portion of the SPM

In May 2017, a part of SPM has been set up to work in islanded configuration and analysed in terms of stability, power quality and load sharing. The SPM islanded portion is connected to two different LV buses, namely Q1 and Q2 connected by means of a 150 m LV cable (as depicted in Fig. 3). The rest of the SPM and the main distribution grid is disconnected by the islanded portion of the SPM. The islanded SPM includes the following elements:

- N.1 Sodium-Nickel ST unit manufactured by FIAMM and characterized by 141 kWh energy capacity and 62 kVA rated power connected to bus Q2 (Fig. 4a);
- N.3 aggregated PV power plants each characterized by 5 kWp rated power (for a total of 15 kWp) connected to bus Q1 by means of a LV cable, from now on PV1 (Fig. 4b);
- N.1 77 kWp PV plant connected to bus Q2, from now on PV2 (Fig. 4c);
- One building of the Savona Campus connected to bus Q1 behaving like a passive load characterized by a rated power of 20 kW; This load is characterized by a stochastic behaviour due to the activities ongoing in the building;
- An adjustable resistive symmetric load connected to bus Q2, rated power of 10kW. This load is used to simulate load variations in a controllable way (see Fig. 4d).

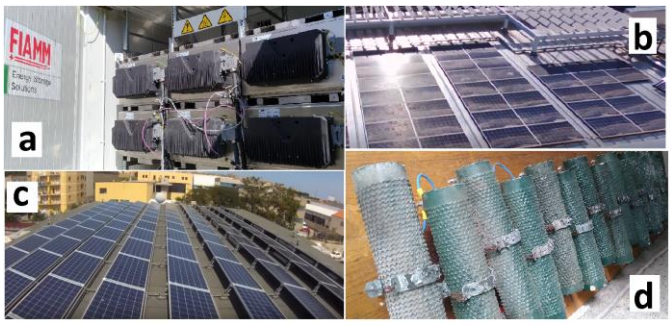

Fig. 4. a) FIAMM storage; b) PV1 generating unit; c) PV2 generating unit; d) adjustable load

On the basis of the description provided above, the load is composed by an uncontrollable (and unbalanced) portion due to the power absorption of the building and a controllable one represented by the set of variable resistors. The islanded SPM is controlled by means of a master/slave logic [26] where the ST is the master (slack node), and the PVs are the slaves (PQ nodes) [3, 27, 28]. The ST inverter is in charge of providing a frequency reference accounting for the voltage regulation at its terminals and guaranteeing the system power balance.

IV. PSCAD Model

Beside the validation on the SPM experimental test bed, the proposed SM has also been compared against an implementation of the islanded portion of the SPM on PSCAD-EMTDC, a commercial software for electromagnetic simulation. This comparison is done in order to have a simulative reference for the proposed SM accounting for a more accurate dynamic of electrical quantities. Implementation on an electromagnetic simulator allows accounting for higher order dynamics of the system in order to evaluate the impact of the SM hypotheses on the final result.

The main differences between the PSCAD model and the proposed SM are: *(i)* all electronic devices (DC/DC and

DC/AC) consist of controlled not ideal IGBT with PWM modulation and *(ii)* each inverter has an AC filter composed with a series and a shunt section in order to suppress the PWM harmonics, as depicted in Fig. 5.

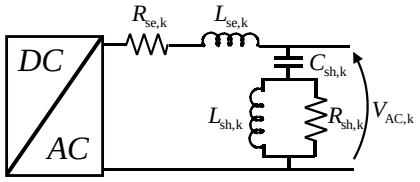

Fig. 5. Inverter AC filter implemented in PSCAD

Under these assumptions, the whole harmonic spectrum is accounted both on the DC and AC side in the PSCAD environment. As far as the PV systems and the ST unit are concerned, they have been implemented by the authors as a DC bipole connected to the DC side of the corresponding converter section. The PV one accounts for (8) while the ST one includes (10), (11) and (12).

V. Test Case Parameter Definition

Before starting with the experimental validation of the proposed SM, it is necessary to characterize all the parameters needed to set up the SM in a suitable environment. For the following simulations the SM has been implemented in MATLAB. With reference to the SM general formulation of Section II, for the specific case of the islanded portion of the SPM N is equal to three, N_{ST} is one and N_{PV} is equal to two. Using the same structure depicted in Fig. 1, it is possible to include in the extended admittance matrix all the loads and the elements of the AC side of each power generating unit. Fig. 6 depicts the system one line diagram.

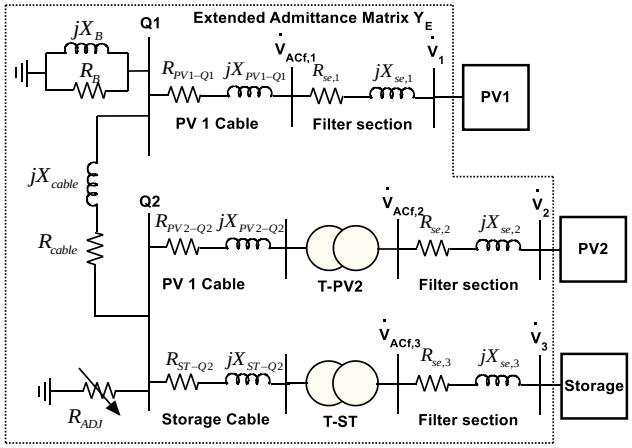

Fig. 6. SPM islanded section one-line diagram.

As one can see, both PV2 and the ST system are equipped with a dedicated transformer and a cable connection is present for every generating unit to connect busses Q1 and Q2. In the proposed implementation, cables are modelled by means of a simple resistive-inductive series impedance, suitable at the light of the reduced length of the cables, and transformers are represented with the only leakage reactance. All the parameters of the test bed AC network are reported in TABLE I.

TABLE I – Test bed facility AC section parameters

$R_{se,1}$	0.314 mΩ	R_{PV2-Q2}	0.0208 Ω
$X_{se,1}$	0.314 Ω	X_{PV2-Q2}	0.0044 Ω
R_{PV1-Q1}	0.057 Ω	$R_{se,3}$	0.314 mΩ
X_{PV1-Q1}	1.027 Ω	$X_{se,3}$	0.314 Ω
$R_{se,2}$	0.314 mΩ	X_{T-ST}	0.0088 Ω
$X_{se,2}$	0.314 Ω	R_{ST-Q2}	0.0435 Ω
X_{T-PV2}	0.137 Ω	X_{ST-Q2}	0.0039 Ω

The PV parameters necessary to implement (8) are the same for the two PV plants and are detailed in TABLE II. The solar irradiance has been calculated in order to fit the real system measurement at the initial steady-state, due to the absence of a dedicated solar irradiance meter.

TABLE II – PV1 and PV2 systems parameters

TC_I	0.06 °C-1	α_{min}	200 W/m2
TC_V	-0.31 °C-1	α_{max}	1000 W/m2
I_{SC}	8.75 A	α	800 W/m2
b	0.0777 -	T	25 °C
v_{min}	35 V	C_1	2.5 mF
v_{max}	37.11 V	C_2	2.5 mF

The ST needs to be characterized providing the coefficients of (10) in addition to its internal resistance, the DC capacitance and NCC (data are included in TABLE III and TABLE IV).

TABLE III – Equivalent ST internal voltage coefficients

a_6	a_5	a_4	a_3	a_2	a_1	a_0
$4 \cdot 10^{-9}$	$-1 \cdot 10^{-3}$	$2 \cdot 10^{-4}$	$-8 \cdot 10^{-3}$	0.1	13	600

TABLE IV – ST system parameters

$R_{int,3}$	$L_{st,3}$	NCC_3	C_3
1.1205 Ω	1 mH	228 Ah	3 mF

Finally, attention must be paid to the load characterization, especially to the building one. As stated in Section II, in the SM, the load is represented by an algebraic voltage/current law. Since the building load is characterized by a stochastic behaviour, the first problem to be faced is to find out a possible closed-form law that fits with the real behaviour. As a first comment, no motors or large under converter loads are present in the building, since it only hosts classes and offices (heating and cooling are provided by a central station which is not electrically connected to the islanded SPM). This suggests the possibility of considering a linear law (i.e. to suppose that the building load can be represented by a resistance and a reactance posed in parallel). Of course, a specific validation of this assumption is not possible, but the agreement between simulation results and measurements will give a justification of this choice. In order to calculate the suitable value of the building equivalent resistance and reactance, the following procedure has been derived. If one neglects distribution losses, the active and reactive power absorbed by the building load (P_{LOAD} and Q_{LOAD}) can be estimated from the active and reactive power delivered at the ST AC terminals, $P_{AC,3}$ and $Q_{AC,3}$ in addition to the active and reactive power injected by each PV unit, $P_{AC,2(1)}$ and $Q_{AC,2(1)}$:

$$\begin{cases} P_{LOAD} = P_{AC,1} + P_{AC,2} + P_{AC,3} \\ Q_{LOAD} = Q_{AC,1} + Q_{AC,2} + Q_{AC,3} \end{cases} \quad (15)$$

Assuming that the system voltage drop is negligible, due to the limited length of all connecting cables, the voltage at bus 2 can be assumed equal to the ST one ($V_{AC,3}$). It is then possible to calculate the equivalent building load phase resistance and reactance R_B and X_B as:

$$R_B = \frac{3V_{AC,3}^2}{P_{LOAD}}, X_B = \frac{3V_{AC,3}^2}{Q_{LOAD}} \quad (16)$$

In the considered case, the numerical values of the equivalent building load phase resistance (R_B) and reactance (X_B) are 13.2 Ω and 33 Ω respectively (corresponding to an active and

reactive power absorption of about 12 kW and 4.8 kVAr). In addition to the parameter list up to now, the PSCAD model needs a wider set of data, since it also includes the shunt section of the inverter AC filters. The PSCAD model additional data are grouped in TABLE V (identical for the three units).

TABLE V – PSCAD additional parameters

$R_{sh,1}=R_{sh,2}=R_{sh,3}$	$L_{sh,1}=L_{sh,2}=L_{sh,3}$	$C_{sh,1}=C_{sh,2}=C_{sh,3}$
2.615 kΩ	0.0166 mH	1 μF

As pointed out in Section II, the specific control logic is out of the scope of the present article; nevertheless, in order to compare the results obtained by the experimental validation and the simulation ones, the islanded SPM control strategy needs to be implemented in both the models. The islanded SPM accounts for a master/slave control where the ST is the master unit providing the frequency reference to the system and regulating its terminal voltage. The slave units, PV1 and PV2, are regulated on the basis of an active and reactive power independent reference and they are locked to the measured system frequency. As a consequence, the master unit guarantees the electric power balance. The PVs active power reference is provided by a minimum logic selection between the signal of the MPP and the eventual active power external limitation. As outputs, the master/slave control logic provides the frequency and modulation index for the master unit and the modulation index and the phase shift for the slave ones.

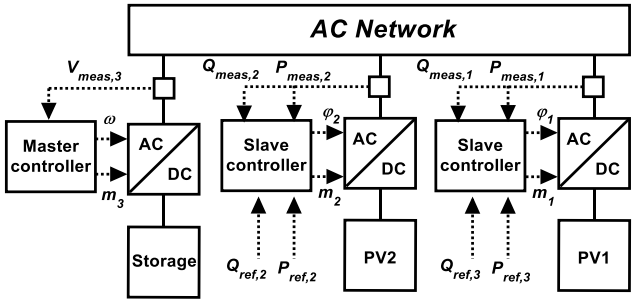

Fig. 7. SPM island control logic

The master/slave control logic of the islanded portion of the SPM is sketched in Fig. 7. This philosophy has been implemented in both models in order to achieve consistent results. The Master controller aims at keeping the ST AC voltage after the filtering section $V_{ACf,3}$ at its rated value acting on the modulation index m_3 by means of a Proportional Integral (PI) controller, as depicted in Fig. 8 while the modulation function phase is fixed at zero. The master controller also imposes the system frequency ω.

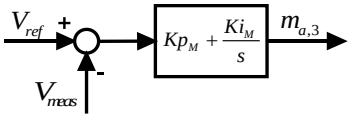

Fig. 8. Master unit control scheme

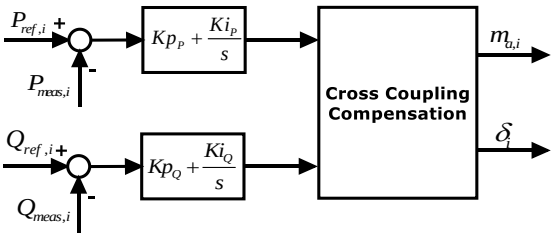

Fig. 9. Slave units control scheme

The slave controllers provide active and reactive power control in accordance to specific reference signals (e.g. for the PV systems the MPP signal and the reactive power external reference). The controller accounts for two PI controllers and a cross coupling compensation as depicted in Fig. 9 for the generic *i-th* slave unit (see [29] for details).

VI. EXPERIMENTAL VALIDATION

The aim of this section is to provide a validation of the proposed MG model. As previously highlighted, the validation has been performed comparing the results obtained by the proposed SM with the ones of a detailed time domain simulation implemented in PSCAD environment and against on-field measurement acquired at the University of Genoa SPM test bed facility. To achieve the target of acquiring a complete set of meaningful data, two different measurement instruments were used, both posed downstream of the ST inverter and transformer. The first one is a Jupiter Power Quality Analyser [30], while the second is a Fluke 190-104 ScopeMeter [31]. The Jupiter Power Quality is used to acquire the measurement of the values of current, voltage and power on a wider horizon due to its capability to sample one value per second. The Fluke 190-104 ScopeMeter, on the other hand, is capable of showing voltages and currents waveforms in a precise way and was used to record phase currents and voltages waveforms in a narrow temporal window thanks to its 160 μs sampling time. The comparison is made considering the ST active power, the AC line to ground voltage and the AC phase current. However, since the Jupiter Power Quality Analyzer sampling time is in the order of one point per second, it is not capable of providing a suitable measurement for an accurate comparison. For this reason, active and reactive power have been calculated on the basis of the ST current and voltage waveforms recorded by the Fluke oscilloscope applying the well-known instantaneous power theory in the Park domain [29]. The comparison is performed accounting for three different scenarios representative of possible occurrences in the MG operation, corresponding to a load variation (Scenario A), a reactive power reference variation (Scenario B) and a PV unit disconnection (Scenario C). For the three scenarios, PV units were limited in power production in order to avoid errors introduced by possible power variation due to unpredicted irradiance changes during the measurement period. The SPM initial operational condition is summarized in Table VI.

TABLE VI – Initial MG steady-state condition

Component	Active power	Reactive power
PV1	9 kW	0 kVAr
PV2	20 kW	0 kVAr
ST	-16.8 kW	5.0 kVA
Load	about 12 kW	about 4.8 kVAr
Resistor load	0 kW	0 kVAr

A. Scenario A – Load variation

The first test case scenario aims at highlighting the performances of the SM after a load variation. The load variation is simulated in a deterministic way inserting the additional resistor bank after 1 s from the beginning of the data acquisition with an equivalent power request increase equal to 10 kW. As one can see from Fig. 10, the ST active power absorption decreases and this is confirmed by the reduction of its AC current (see first sub-plot of Fig. 11), where the current peak passes from about 35 A to 20 A. in particular, the active

This article has been accepted for publication in a future issue of this journal, but has not been fully edited. Content may change prior to final publication. Citation information: DOI 10.1109/TSTE.2018.2816401, IEEE Transactions on Sustainable Energy

power variation recorded at the ST terminals is 10.4 kW, showing that this component satisfies the load increased demand together with losses compensation. The AC ST voltage (second sub-plot of Fig. 11) does not suffer the load variation keeping mainly constant its peak value.

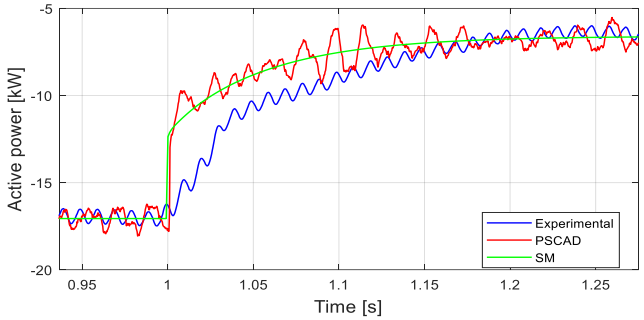

Fig. 10. Scenario A ST active power. Experimental data (blue line), PSCAD (red line) and SM (green line).

All the figures exhibit a good agreement among the curves both for steady-state and transient. The most relevant difference among the simplified and PSCAD models and the experimental results can be seen in Fig. 10, where both the models active powers reach the final steady-state before the measured one.

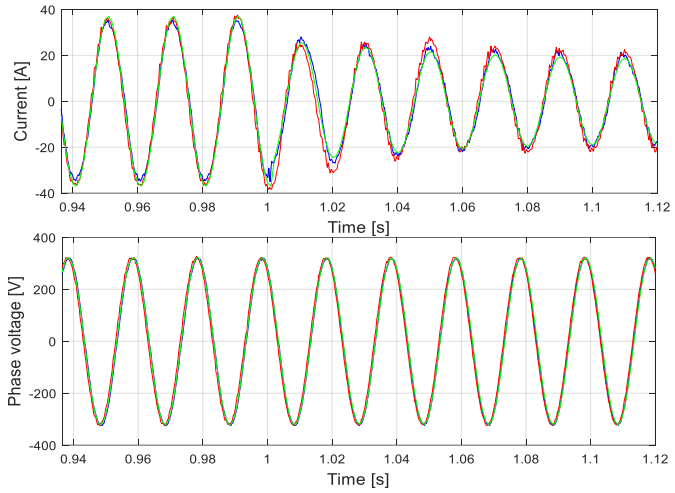

Fig. 11. Scenario A ST current and phase voltage. Experimental data (blue line), PSCAD (red line) and SM (green line).

This is due to the fact that, as the inverter controller and filter details have not been shared by the manufacturer, typical topologies, parameters and control strategies have been assumed in the models in order to achieve the best possible fitting.

B. Scenario B - Reactive power variation

The second test case concerns a reactive power variation of PV2 unit. Starting from the initial condition of Table VI, a step variation of the reactive power reference is provided to PV2 inverter, passing from 0 to -10 kVAr. The experimental recording of Fig. 12 (blue curve) highlights that the ST reactive power follows the step reference with a sensible delay. This is probably due to a rate limiter included in the PV internal controller, whose details have not been shared by the manufacturer. For this reason, in order to mimic the experimental conditions for the two models, a rate limiter has been implemented in both models whose parameters have been guessed in order to reach a good fitting with experimental results. The comparison appears in in Fig. 12 highlighting an excellent agreement concerning steady-state values and some slight deviations during the transient. Finally, Fig. 13 shows the good agreement among the three curves in terms of current and phase voltage waveforms at the AC side of the inverter.

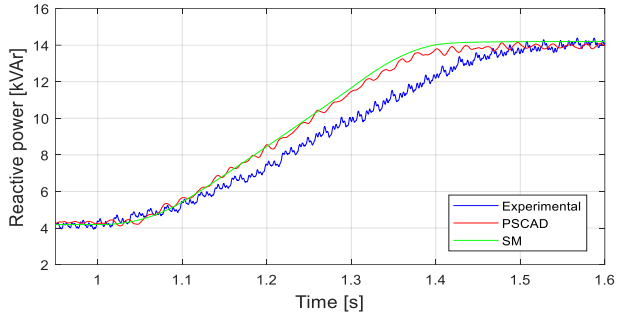

Fig. 12. Scenario B ST reactive power. Experimental data (blue line), PSCAD (red line) and SM (green line).

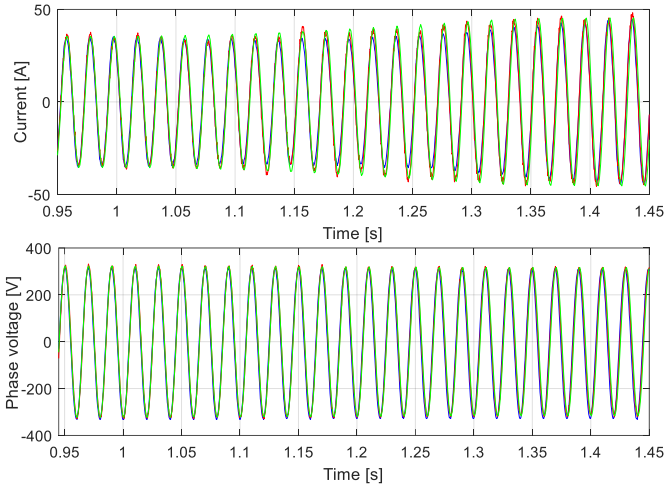

Fig. 13. Scenario B ST current and phase voltage. Experimental data (blue line), PSCAD (red line) and SM (green line).

C. Scenario C - PV2 disconnection

PV2 disconnection (after 1 s from the beginning of data acquisition) is representative of a clouding or a disconnection subsequent to a fault or an overloading of the PV system. In the SM the PV2 disconnection can be simulated zeroing the line and the column of the admittance matrix corresponding to its bus. The initial steady-state for Scenario C is a little different from test cases A and B because the controllable resistive bank was fully inserted in the initial steady-state. This variation has been introduced to obtain a ST dynamics characterized by a power flow inversion in order to validate the model in both the ST operational conditions (power production and absorption) and during the transition between different assets. For this reason, the initial ST power production is equal to -6.8 kW. The first sub-plot of Fig. 14 describes the behaviour of the ST phase current when PV2 is detached. As one can see, the current increases its amplitude and has a phase shifting so that the active power request by the load is satisfied. Moreover, in Fig. 15 one can notice the active power inversion at the ST AC bus bar. The agreement among the two approaches is still good with some deviations with experimental data in the power sign inversion transient, partially due to the lack of information on the inverter and chopper controllers. The second sub-plot of

This article has been accepted for publication in a future issue of this journal, but has not been fully edited. Content may change prior to final publication. Citation information: DOI 10.1109/TSTE.2018.2816401, IEEE Transactions on Sustainable Energy

Fig. 14 describes the voltage behaviour, which is again not affected by the contingency.

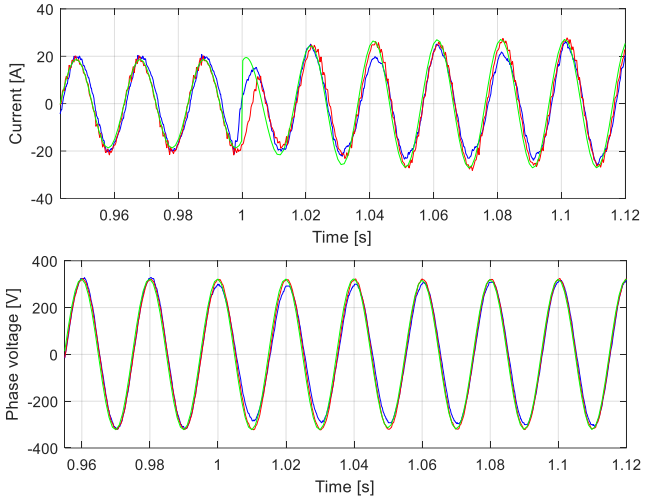

Fig. 14. Scenario C ST current and phase voltage. Experimental data (blue line), PSCAD (red line) and SM (green line).

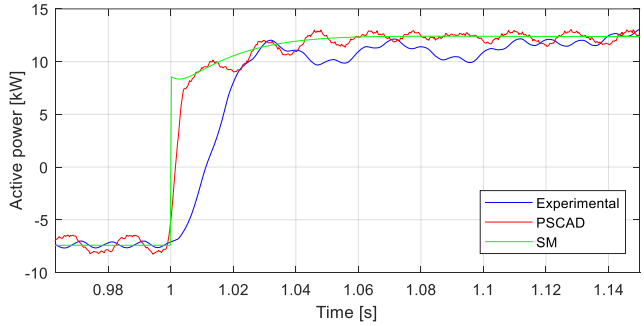

Fig. 15. Scenario C ST active power. Experimental data (blue line), PSCAD (red line) and SM (green line).

In conclusion, the experimental campaign shows that the proposed SM is in good agreement with the measurements and the PSCAD simulation, with some minor differences that can be mainly ascribed to the following reasons. Firstly, the load is unknown due to its stochastic behaviour and it cannot be directly measured due to SPM actual layout. Secondly, inverter and DC-DC converter internal controller details and computational delays are not precisely known (modulation strategy, carrier frequency, filters data and so on) since the producer did not share detailed information. Finally, the electrochemical dynamics in the ST system are not taken into account in the SM and PSCAD one. Nevertheless, the results allow considering the SM sufficiently reliable to be implemented for the validation and preliminary test of innovative control strategies and EMS for islanded no-inertia MGs. In particular, the SM ODE could constitute the set of constraints for a Model Predictive Controller (MPC) aimed at regulating the MG voltages and frequency. The flexibility of the structure of the SM allows extending it at different assets of MGs characterized by a heterogeneous generation mix.

VII. Conclusions

This paper aimed at providing an experimental validation of a modelling approach to study the behaviour of no-inertia MGs in islanded configuration. Such model describes the MG with a system of ODEs representing a first harmonic dynamics of the power electronic devices and of all the components at the DC converters side. The coupling among the various MG components is achieved by means of a steady-state representation of the AC section of the MG using the extended admittance matrix. The main advantage of the SM is that it can be easily interfaced with many different control logics in order to provide a preliminary evaluation of the controller expected performances in an easy but effective way, reducing the commissioning cost. The proposed model has been validated against a detailed simulation in the PSCAD-EMTDC environment and with data acquired during a measurement campaign on a portion of the SPM islanded from the rest of the campus grid. Results highlighted a good trade-off between accuracy and computational effort, suitable for a first evaluation of innovative control approaches. Further developments will include the validation of the proposed models also under fault conditions in order to study the possible use of the model for the design and coordination of protection devices in no-inertia MGs.

VIII. Appendix

A. Load voltage dependent extended admittance matrix

Let us consider an AC network characterized by N_b buses. Moreover let $N_b=N+N_L$, being N_L the number of load buses. For the future development, one can express the voltage and current vectors as follows:

$$\begin{cases}\dot{\mathbf{V}}=\left[\dot{\mathbf{V}}_L^{\,T}\quad\dot{\mathbf{V}}_S^{\,T}\right]^T\\ \dot{\mathbf{I}}=\left[\dot{\mathbf{I}}_L^{\,T}\quad\dot{\mathbf{I}}_S^{\,T}\right]^T\end{cases}\tag{A.1}$$

being $\left[\dot{\mathbf{V}}_L\right]=\left[\dot{V}_{L1}..\dot{V}_{LN}\right]^T$ ($\left[\dot{\mathbf{I}}_L\right]=\left[\dot{I}_{L1}..\dot{I}_{LN}\right]^T$) and $\left[\dot{\mathbf{V}}_S\right]=\left[\dot{V}_1..\dot{V}_N\right]^T$ ($\left[\dot{\mathbf{I}}_S\right]=\left[\dot{I}_1..\dot{I}_N\right]^T$) the load and source voltage (current) vectors respectively. With this approach, the network admittance matrix $\mathbf{Y}$ can be partitioned as follows:

$$\mathbf{Y}=\begin{bmatrix}\mathbf{Y}_{LL}&\mathbf{Y}_{LS}\\ \mathbf{Y}_{SL}&\mathbf{Y}_{SS}\end{bmatrix}\tag{A.2}$$

such that:

$$\begin{cases}\left[\dot{\mathbf{I}}_S\right]=\left[\mathbf{Y}_{SL}\right]\left[\dot{\mathbf{V}}_L\right]+\left[\mathbf{Y}_{SS}\right]\left[\dot{\mathbf{V}}_S\right]\\ \left[\dot{\mathbf{I}}_L\right]=\left[\mathbf{Y}_{LL}\right]\left[\dot{\mathbf{V}}_L\right]+\left[\mathbf{Y}_{LS}\right]\left[\dot{\mathbf{V}}_S\right]\end{cases}.\tag{A.3}$$

Assuming that the loads are described with an algebraic law of the kind:

$$\dot{I}_{Li}=\dot{I}_{Li}\left(\dot{V}_{Li}\right)\quad i=1..N_L\tag{A.4}$$

it is possible defining:

$$\dot{y}_{Li}\left(\dot{V}_{Li}\right)=\frac{\dot{I}_{Li}\left(\dot{V}_{Li}\right)}{\dot{V}_{Li}}\quad i=1..N_L\tag{A.5}$$

and:

$$\mathbf{Y}_L\left(\left[\dot{\mathbf{V}}_L\right]\right)=diag\left(y_{Li}\left(\dot{V}_{Li}\right)\right)\tag{A.6}$$

So, it readily follows that for any load bus:

$$\left[\dot{\mathbf{I}}_L\right]=\left[\mathbf{Y}_L\left(\left[\dot{\mathbf{V}}_L\right]\right)\right]\left[\dot{\mathbf{V}}_L\right]\tag{A.7}$$

Then, combining (A.7) and (A.3), one has:

$$\left[\dot{\mathbf{V}}_L\right]=-\left[\mathbf{Y}_L\left(\left[\dot{\mathbf{V}}_L\right]\right)+\mathbf{Y}_{LL}\right]^{-1}\left[\mathbf{Y}_{LS}\right]\left[\dot{\mathbf{V}}_S\right]\tag{A.8}$$

and

$$\left[\dot{\mathbf{I}}_S\right] = -\left[\mathbf{Y}_{SL}\right]\left[\mathbf{Y}_L\left(\left[\dot{\mathbf{V}}_L\right]\right) + \mathbf{Y}_{LL}\right]^{-1}\left[\mathbf{Y}_{LS}\right]\left[\dot{\mathbf{V}}_S\right] + \\ + \left[\mathbf{Y}_{SS}\right]\left[\dot{\mathbf{V}}_S\right] = \left[\mathbf{Y}_e\left(\left[\dot{\mathbf{V}}_L\right]\right)\right]\left[\dot{\mathbf{V}}_S\right] \quad \text{(A.9)}$$

having defined

$$\left[\mathbf{Y}_e\left(\left[\dot{\mathbf{V}}_L\right]\right)\right] = \mathbf{Y}_{SS} - \left[\mathbf{Y}_{SL}\right]\left[\mathbf{Y}_L\left(\left[\dot{\mathbf{V}}_L\right]\right) + \mathbf{Y}_{LL}\right]^{-1}\left[\mathbf{Y}_{LS}\right]. \quad \text{(A.10)}$$

B. Numerical solution of the ODE system of the MG dynamics

In order to describe the dynamic behaviour of the microgrid according to the proposed SM, one has to solve the ODEs system (2)-(3) and (5)-(14).

Unfortunately, the dependence of the extended admittance matrix on the load voltage vector does not allow to state the system in the normal form (which is necessary for the implementation on any numerical simulator). In other words, (A.8)-(1) represent an implicit functional relationship between the state variables and the load voltage that cannot be solved analytically. In order to circumvent this problem, one can proceed as follows: suppose that at time t_n the system state vector is known; consequently, the knowledge of the DC side voltages of all the inverters allows finding the entries of $\left[\dot{\mathbf{V}}_S\left(t_n\right)\right]$ at time t_n. Then, the application of the fixed point method allows updating the load voltage vector and the extended network admittance matrix as follows:

$$\left[\dot{\mathbf{V}}_L\left(t_{n+1}\right)\right] = -\left[\mathbf{Y}_L\left(\left[\dot{\mathbf{V}}_L\left(t_n\right)\right]\right) + \mathbf{Y}_{LL}\right]^{-1}\left[\mathbf{Y}_{LS}\right]\left[\dot{\mathbf{V}}_S\left(t_n\right)\right] \quad \text{(A.11)}$$

$$\left[\mathbf{Y}_e\left(\left[\dot{\mathbf{V}}_L\left(t_{n+1}\right)\right]\right)\right] = \mathbf{Y}_{SS} + \\ -\left[\mathbf{Y}_{SL}\right]\left[\mathbf{Y}_L\left(\left[\dot{\mathbf{V}}_L\left(t_{n+1}\right)\right]\right) + \mathbf{Y}_{LL}\right]^{-1}\left[\mathbf{Y}_{LS}\right] \quad \text{(A.12)}$$

Consequently, the state vector at time t_{n+1} is calculated using (2)-(3) and (5)-(14). Such iterative procedure can obviously be initialized having at disposal the results of the initial load flow.

REFERENCES

[1] S. Aman, Y. Simmhan, and V. K. Prasanna, "Energy management systems: State of the art and emerging trends," *IEEE Community Magazine*, vol. 51, pp. 114-119, 2013.

[2] S. Bracco, M. Brignone, F. Delfino, and R. Procopio, "An Energy Management System for the Savona Campus Smart Polygeneration Microgrid," *IEEE Systems Journal*, vol. PP, pp. 1-11, 2015.

[3] A. Davoudi and A. Bidram, "Hierarchical Structure of Microgrids Control System," *IEEE Transactions on Smart Grid*, vol. 3, 2012.

[4] J. M. Guerrero, J. Matas, G. Vicuna, J. Miret, and M. Castilla, "Decentralized Control for Parallel Operation of Distributed Generation Inverters in Microgrids Using Resistive Output Impedance," *IEEE Transaction on Industrial Applications*, vol. 54, 2007.

[5] J. Sachs and O. Sawodny, "A Two-Stage Model Predictive Control Strategy for Economic Diesel-PV-Battery Island Microgrid Operation in Rural Areas," *IEEE Transactions on Sustainable Energy*, vol. 7, pp. 903-913, 2016.

[6] B. Singh, G. Pathak, and B. K. Panigrahi, "Seamless Transfer of Renewable based Microgrid between Utility Grid and Diesel Generator," *IEEE Transactions on Power Electronics*, vol. PP, pp. 1-1, 2017.

[7] A. Hooshyar and R. Iravani, "Microgrid Protection," *Proceedings of the IEEE*, vol. 105, pp. 1332-1353, 2017.

[8] H. Han, X. Hou, J. Yang, J. Wu, M. Su, and J. M. Guerrero, "Review of Power Sharing Control Strategies for Islanding Operation of AC Microgrids," *IEEE Transactions on Smart Grid*, vol. 7, pp. 200-215, 2016.

[9] X. Tang, X. Hu, N. Li, W. Deng, and G. Zhang, "A Novel Frequency and Voltage Control Method for Islanded Microgrid Based on Multienergy Storages," *IEEE Transactions on Smart Grid*, vol. 7, pp. 410-419, 2016.

[10] A. Bonfiglio, F. Delfino, M. Invernizzi, R. Procopio, and P. Serra, "An approximate methodology to verify the compliance of large photovoltaic power plants to system operator steady-state requirements," *Electric Power Systems Research*, vol. 127, pp. 80-92, 2015.

[11] A. Bonfiglio, F. Delfino, M. Invernizzi, A. Labella, D. Mestriner, R. Procopio, *et al.*, "Approximate characterization of large Photovoltaic power plants at the Point of Interconnection," in *Proceedings of the Universities Power Engineering Conference*, 2015.

[12] M. Rasheduzzaman, J. A. Mueller, and J. W. Kimball, "Reduced-Order Small-Signal Model of Microgrid Systems," *IEEE Transactions on Sustainable Energy*, vol. 6, pp. 1292-1305, 2015.

[13] X. Guo, Z. Lu, B. Wang, X. Sun, L. Wang, and J. M. Guerrero, "Dynamic Phasors-Based Modeling and Stability Analysis of Droop-Controlled Inverters for Microgrid Applications," *IEEE Transactions on Smart Grid*, vol. 5, pp. 2980-2987, 2014.

[14] A. M. Stankovic, B. C. Lesieutre, and T. Aydin, "Modeling and analysis of single-phase induction machines with dynamic phasors," *IEEE Transactions on Power Systems*, vol. 14, pp. 9-14, 1999.

[15] S. Augustine, M. K. Mishra, and N. Lakshminarasamma, "Adaptive Droop Control Strategy for Load Sharing and Circulating Current Minimization in Low-Voltage Standalone DC Microgrid," *IEEE Transactions on Sustainable Energy*, vol. 6, pp. 132-141, 2015.

[16] S. Chakraborty and M. G. Simoes, "Experimental Evaluation of Active Filtering in a Single-Phase High-Frequency AC Microgrid," *IEEE Transactions on Energy Conversion*, vol. 24, pp. 673-682, 2009.

[17] F. Guo, H. Li, C. Yao, M. Alsolami, A. Lang, X. Lu, *et al.*, "Residential usage profile optimization and experimental implementation of the retired HEV battery with a hybrid microgrid testbed," in *2014 IEEE Energy Conversion Congress and Exposition (ECCE)*, 2014, pp. 428-435.

[18] L. Yunwei, D. M. Vilathgamuwa, and L. Poh Chiang, "Design, analysis, and real-time testing of a controller for multibus microgrid system," *IEEE Transactions on Power Electronics*, vol. 19, pp. 1195-1204, 2004.

[19] Manitoba-HVDC. *PSCAD Library*. Available: https://hvdc.ca/knowledge-library/reference-material

[20] R. Erickson and D. Maksimovic, *Fundamentals of Power Electronics,2nd edition*: Kluwer Academic, 2004.

[21] A. Bonfiglio, F. Delfino, M. Invernizzi, and R. Procopio, "Modeling and Maximum Power Point Tracking Control of Wind Generating Units Equipped with Permanent Magnet Synchronous Generators in Presence of Losses," *Energies*, vol. 10, p. 102, 2017.

[22] I. Bendato, A. Bonfiglio, M. Brignone, F. Delfino, F. Pampararo, and R. Procopio, "A real-time Energy Management System for the integration of economical aspects and system operator requirements: Definition and validation," *Renewable Energy*, vol. 102, pp. 406-416, 2017.

[23] U. Boke, "A simple model of photovoltaic module electric characteristics," in *2007 European Conference on Power Electronics and Applications*, 2007, pp. 1-8.

[24] A. Labella, D. Mestriner, R. Procopio, and F. Delfino, "A simplified first harmonic model for the Savona Campus Smart Polygeneration Microgrid," in *2017 IEEE International Conference on Environment and Electrical Engineering and 2017 IEEE Industrial and Commercial Power Systems Europe (EEEIC / I&CPS Europe)*, 2017, pp. 1-6.

[25] A. Bonfiglio, F. Delfino, F. Pampararo, R. Procopio, M. Rossi, and L. Barillari, "The Smart Polygeneration Microgrid test-bed facility of Genoa University," in *2012 47th International Universities Power Engineering Conference (UPEC)*, 2012, pp. 1-6.

[26] C. Yeong Jia and E. K. K. Sng, "A novel communication strategy for decentralized control of paralleled multi-inverter systems," *IEEE Transactions on Power Electronics*, vol. 21, pp. 148-156, 2006.

[27] Y. Han, H. Li, P. Shen, E. A. A. Coelho, and J. M. Guerrero, "Review of Active and Reactive Power Sharing Strategies in Hierarchical Controlled Microgrids," *IEEE Transactions on Power Electronics*, vol. 32, pp. 2427-2451, 2017.

[28] J. M. Guerrero, "Hierarchical control of droop-controlled AC and DCmicrogrids—A general approach toward standardization," *IEEE Transactions on Industrial Electronics*, Jan. 2011.

[29] F. Milano, *Power system modelling and scripting*: Springer Science & Business Media, 2010.

[30] DuncanInstruments. Available: duncaninstr.com/Jupiter.htm

[31] Fluke. Available: fluke.com/products/portable-oscilloscopes/fluke-190-ii-portable-oscilloscope-190-104-s.html